

LOW-ORDER MODELLING OF DUCTED FLAMES WITH TEMPORALLY VARYING EQUIVALENCE RATIO IN REALISTIC GEOMETRIES

Owen S. Graham *

Ann P. Dowling

Acoustics Laboratory

Department of Engineering

Cambridge University, Trumpington Street, Cambridge, CB2 1PZ, UK

Email: og232@cam.ac.uk,

ABSTRACT

The interaction between unsteady heat release and acoustic pressure oscillations in gas turbines results in self-excited combustion oscillations which can potentially be strong enough to cause significant structural damage to the combustor. Correctly predicting the interaction of these processes, and anticipating the onset of these oscillations can be difficult. In recent years much research effort has focused on the response of premixed flames to velocity and equivalence ratio perturbations.

In this paper, we develop a flame model based on the so-called G-Equation, which captures the kinematic evolution of the flame surfaces, under the assumptions of axisymmetry, and ignoring vorticity and compressibility. This builds on previous work by Dowling [1], Schuller et al. [2], Cho & Lieuwen [3], among many others, and extends the model to a realistic geometry, with two intersecting flame surfaces within a non-uniform velocity field. The inputs to the model are the free-stream velocity perturbations, and the associated equivalence ratio perturbations. The model also proposes a time-delay calculation wherein the time delay for the fuel convection varies both spatially and temporally. The flame response from this model was compared with experiments conducted by Balachandran [4, 5], and found to show promising agreement with experimental forced case.

To address the primary industrial interest of predicting self-excited limit cycles, the model has then been linked with an acoustic network model to simulate the closed-loop interaction

between the combustion and acoustic processes. This has been done both linearly and nonlinearly. The nonlinear analysis is achieved by applying a describing function analysis in the frequency domain to predict the limit cycle, and also through a time domain simulation. In the latter case, the acoustic field is assumed to remain linear, with the nonlinearity in the response of the combustion to flow and equivalence ratio perturbations. A transfer function from unsteady heat release to unsteady pressure is obtained from a linear acoustic network model, and the corresponding Green function is used to provide the input to the flame model as it evolves in the time domain. The predicted unstable frequency and limit cycle are in good agreement with experiment, demonstrating the potential of this approach to predict instabilities, and as a test bench for developing control strategies.

Keywords: Combustion Instabilities, G-Equation, Thermoacoustics, Gas Turbines, Premixed Flames.

NOMENCLATURE

- A Amplitude of the velocity perturbation, normalised
- a Downstream radius of the bluff body flame holder
- b Outer radius of inflow annulus
- c Radius of combustor
- d Inner radius of inflow annulus
- H Flame Transfer Function between u'/\bar{u} and Q'/\bar{Q}
- ΔH Enthalpy of combustion
- L Distance below dump plane of the source of the spreading flow field

* Address all correspondence to this author.

- L_{inj} Distance from the fuel injection point to the dump plane
 P Velocity potential
 r Radial coordinate
 S_u Flame speed
 u Axial flow velocity
 u_0 Magnitude of flow velocity at fuel injection point
 u_G Average magnitude of flow velocity at the entrance to the combustor
 v Radial flow velocity
 V Forcing amplitude (% of mean)

Greek Symbols

- α Cone angle of the bluff-body flame holder
 ζ Axial position of outer flame surface
 η Combustion efficiency
 θ Azimuthal coordinate
 ξ Axial position of inner flame surface
 ρ Spherical radius coordinate
 ρ_u Mean density of unburnt mixture of fuel and air
 σ Time delays for ζ flame surface
 τ Time delays for ξ flame surface
 ϕ Equivalence (air/fuel) ratio, 1 for stoichiometric
 ϕ_0 Equivalence ratio at fuel injection point
 ω Forcing frequency (in radians)

Superscripts

- Time averaged mean value
 ' Fluctuating value

Mathematical Operators

- Vector Dot Product (Scalar Product)
- ∇ gradient operator
- $\| \ \|$ Magnitude of a vector

INTRODUCTION

One of the most serious issues hindering the development and operation of modern lean-burn gas turbines is the appearance of combustion instabilities (Candel [6], Lieuwen [7]). The term ‘Combustion instabilities’ generally refers to sustained pressure fluctuations in the combustion chamber, resulting from the coupling between the system acoustics and the unsteady heat release. Understanding this self-excited oscillation requires an understanding of complex linear and nonlinear phenomena such as unsteady heat release, acoustic fluctuations, and the interactions between them. Presently, industrial emphasis is shifting increasingly towards developing lean-burn technologies and reducing emissions, as well as exotic fuel-mixes, which can also increase the susceptibility of a system to these instabilities. Combustion instability affects land-based industrial gas turbine systems (Lieuwen [8]), aeroengines (Giuliani et al. [9]), and other combustion systems such as afterburners (Bloxsidge et al. [10]), rocket motors and domestic and industrial boilers. These problems can lead to long and expensive development and commissioning times. Therefore, there is an obvious interest in devel-

oping low order modelling methods that can predict the onset of combustion oscillations, and can be used as an effective design tool in the development stage.

Combustion instabilities occur because unsteady combustion is an efficient acoustic source (Candel et al. [11], Williams [12]). Since combustors generally tend to be highly resonant cavities, the sound waves generated are reflected from the combustor boundaries and can perturb the combustion further. Combustion unsteadiness also generates entropy and vorticity fluctuations which are convected downstream. Their interaction with a downstream constriction can lead to an upstream propagating acoustic wave. Acoustic perturbations at the fuel and air supplies can lead to equivalence ratio fluctuations, which then convect downstream to the combustion zone, where they cause further fluctuations in heat release. If the phase relationship is suitable (Rayleigh [13]), these linear oscillations may increase in energy until limited by nonlinear effects, and lead to a self-excited oscillation. In this paper we investigate the role of equivalence ratio fluctuations in driving the unsteady combustion in a thermoacoustic feedback loop.

Early investigations of the transfer function of premixed flames by Merk [14] proposed a first order model, which is capable of predicting general trends in the flame response. Further work, notably by Blackshear [15] and Matsui [16] characterised the flame’s behaviour as that of a low-pass filter. Experimental work on the effect of pressure oscillations on premixed flames has been the focus of numerous studies since [17–20]. More recent work includes studies by Birbaud et al. [21] and Durox et al. [22] on confined and unconfined wedge-shaped premixed flames, and by Palies et. al [23] and Fritsche et al. [24] on the dynamics of premixed turbulent flames under influence of swirl. Self-excited oscillations in premixed flames have also been studied by Kopp-Vaughan et al. [25] and Hield et al. [26].

Experimental investigations of the effect of equivalence ratio fluctuations are notably rarer, no doubt due in part to the difficulty in obtaining such fluctuations without accompanying velocity fluctuations. Altay et al. [27] described the dynamics of a flame subjected to equivalence ratio oscillations in a backward-facing step combustor. Auer et al. [28,29] studied the influence of the interaction of equivalence ratio and mass flow fluctuations on flame dynamics, with comparison to a 1D flame model. More recently, Kim et al. [30] investigated the response of a centre-body stabilised flame to equivalence ratio perturbations, while Lee et al. [31] studied the combined effects of flame vortex interactions and equivalence ratio perturbations on self-excited acoustic oscillations.

Due to the limitations of purely empirical models, more rigorously physics-based models using a kinematic description of the flame front have now been proposed by many authors. Fleifil et al. [32] described the dependance of the flame response on a flame Strouhal number defined as $\omega R/S_L$. Ducruix et al. [33] extended this analysis to examine the effect of flame angle.

The work by Schuller et al. [2] on conical flames showed the dynamics to be governed by both a reduced frequency, $\omega_* = \omega R / (S_L \cos \alpha)$, and the flame angle α . Lieuwen [34] found strong correlation of flame response with both flame shape 'type' (M, V, etc.) and ratio of flame length to width, as well as Strouhal number. Dowling [1] also introduced the idea of a flame detaching from a flame holder, to allow for velocity perturbations of the order of mean flow. More recent studies that maintain this form of level-set approach include work by Lieuwen [34] on the nonlinear response of premixed flames, and a study by Palies et al. [35] extending this method to swirling flames.

These models deal with premixed flames subjected to in-flow velocity perturbations, but not fluctuations in equivalence ratio. However, initial experimental and theoretical studies (e.g. Keller [36], Hubbard & Dowling [37, 38]) indicate that, in cases where there are significant equivalence ratio fluctuations, these can actually be the dominant mechanism for unsteady heat release. Lieuwen & Zinn [39] and Candel [6] provide good qualitative descriptions of the time delays associated with the production, convection, and combustion of the equivalence ratio fluctuations, and their role in generating thermoacoustic instabilities. More recently, work by Hemchandra et al. [40], You et al. [41], and Cho & Lieuwen [3] extends the G-equation approach to deal with incident equivalence ratio perturbations. These studies describes both the direct effect of equivalence ratio perturbations on the heat of reaction and flame speed, and also the indirect heat release due to the effect of flame speed on flame surface area.

In this paper the kinematic description of the flame front is extended to a case of multiple intersecting flame surfaces in a more realistic geometry with nonuniform flow. This geometry captures many of the features of the combustion zone in gas-turbine combustors. The importance of the convection time for equivalence ratio fluctuations is investigated, with two time-delay models offered. The resulting unsteady heat and Flame Transfer Function (FTF) predictions are compared with experimental results from Balachandran [5], [4]. The model is then linked with a network model, which describes the linear waves in the system, and can be used to model the closed-loop interaction of the combustion and acoustic processes. The limit cycle frequency and amplitude calculated is then compared with experimental evidence.

DEVELOPMENT OF THE G-EQUATION

In the chosen burner configuration (Fig. 1), the flame dynamics are based on a level-set approach. The flame will be represented by two infinitely thin surfaces, separating the reactants from the products. These flame surfaces correspond to a particular level set (i.e. $G = 0$ of the scalar field G). The surfaces move into the fresh reactants (i.e. $G < 0$) in a direction normal to the local surface. Their propagation velocity relative to the fluid flow is denoted by a flame speed S_u , which is consid-

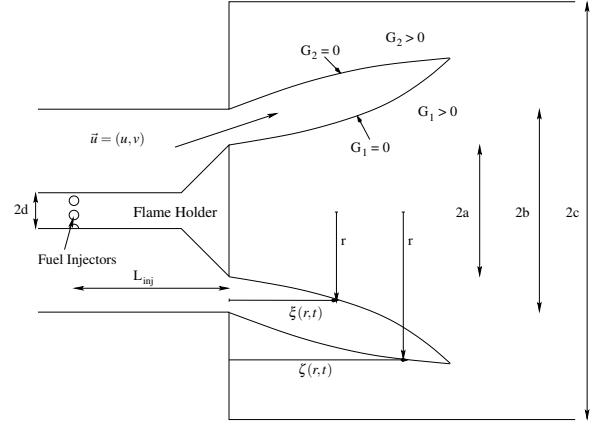


FIGURE 1. SCHEMA OF THE COMPLEX GEOMETRY CASE, FLOW FROM LEFT TO RIGHT, WITH TWO FLAME SURFACES ξ AND ζ

ered to be a function of equivalence ratio. Both compressibility and vorticity across the flame front are ignored, and the model assumes axisymmetry. The flame is stabilised on a conical bluff body, causing the inflow velocity to have both an axial component u , and a radial component v . For the geometry in Fig. 1, consider the arbitrary functions $G_1(z, r, t)$ and $G_2(z, r, t)$, which represent scalar fields defined to be zero at the inner and outer flame fronts, respectively, and positive in the products region. Following Fleifil [32], the equation for the evolution of the flame surfaces can then be written down as follows (written only for G_1 , as second flame surface is identical):

$$\frac{\partial G_1}{\partial t} + \left(\vec{u} - S_u \frac{\nabla \vec{G}_1}{\|\nabla \vec{G}_1\|} \right) \cdot \nabla \vec{G}_1 = 0 \quad (1)$$

Assuming that the function $G_1(z, r, t)$ can be written as $G_1(z, r, t) = z - \xi(r, t)$, and $G_2(z, r, t)$ can be written as $G_2(z, r, t) = \zeta(r, t) - z$, Eqn. (1) can be rewritten in terms of ξ and ζ :

$$\begin{cases} \frac{\partial \xi}{\partial t} = u - v \frac{\partial \xi}{\partial r} - S_u \sqrt{1 + \left(\frac{\partial \xi}{\partial r} \right)^2} \\ \frac{\partial \zeta}{\partial t} = u - v \frac{\partial \zeta}{\partial r} + S_u \sqrt{1 + \left(\frac{\partial \zeta}{\partial r} \right)^2} \end{cases} \quad (2)$$

Note the change in sign of the term including S_u , reflecting the fact that each surface moves towards the fuel-air mixture. The surfaces may theoretically intersect many times, and the model allows for this. Combustion is assumed to only occur along the

surfaces which enclose unburnt fuel-air mixture. These differential equations can be solved numerically to give the instantaneous flame surface positions. The instantaneous heat release is given by the product of the rate at which reactants cross the flow surface and the enthalpy of reaction ΔH . By integrating along the flame, an expression for the total heat release can be found:

$$Q(t) = 2\pi\rho_u\eta \left[\int_a^c S_u(\phi)\Delta H(\phi)r\sqrt{1 + \left(\frac{\partial\xi}{\partial r}\right)^2} dr + \int_b^c S_u(\phi)\Delta H(\phi)r\sqrt{1 + \left(\frac{\partial\zeta}{\partial r}\right)^2} dr \right] \quad (3)$$

where ΔH and the turbulent flame speed S_u are functions of equivalence ratio. The turbulent flame speed is taken to be a constant factor k_0 multiplying the correlation for laminar flame speed $k_1\phi^{k_2}e^{-k_3(\phi-k_4)^2}$ derived by Abu-Orf [42] and used previously by Cho & Lieuwen [3]. The constant k_0 has been adjusted to fit the steady state turbulent flame brush observed in experiments (Fig. 2). This correlation causes the flame speed to approach zero near the lean flammability limit. The flame front then stops propagating into the unburnt mixture, and the heat release falls to zero. There is, however, the assumption that the flame front will always be reignited when the equivalence ratio rises above that limit again. However, given the recirculation of hot gases near the flame holder, this seems reasonable.

Description of the Flow Field

The model requires velocity-field information to calculate the evolution of the flame front. While this information could be provided from experiments, CFD calculations, etc., that would be hard to include in a network model. Instead, since we want to concentrate on the effects of time-varying equivalence ratio on heat release, we take a simple analytical model for the incompressible velocity field between the fuel injection and the flame which conserves continuity, and captures the gross features of the flow. A further important advantage is that the velocity fluctuations of this velocity field are controlled by a single function of time $A(t)$ (see below). This allows a flame model derived using such a velocity field to be easily coupled to a one-dimensional acoustic network model, which provides a single value of perturbation for the inflow velocity.

In order to have a flow field which expands (in this case past a bluff body flame holder), we take the simple case of a point source. Solving Laplace's equation in spherical polar coordinates (see [43] for details), the expressions for the velocity potential in spherical and cylindrical coordinates are found to be:

$$P = \frac{A(t)}{\rho} \quad P = \frac{A(t)}{\sqrt{r^2 + (z+L)^2}} \quad (4)$$

where the virtual origin of the flow field (and the spherical coordinate system) is a distance L below the dump plane. In cylindrical coordinates, this gives the velocity field of the form:

$$\begin{cases} u_r = \frac{-A(t)r}{\sqrt{(r^2+(z+L)^2)^3}} \\ u_z = \frac{-A(t)(z+L)}{\sqrt{(r^2+(z+L)^2)^3}} \\ u_\theta = 0 \end{cases} \quad (5)$$

Equilibrium Position

To solve for the equilibrium position, we set $\frac{\partial\xi}{\partial t} = 0$ and $\frac{\partial\zeta}{\partial t} = 0$. There is found to be a single solution by quadratic formula for Eqn. (2) for each flame surface:

$$\frac{\partial\bar{\xi}}{\partial r}(z,r) = \frac{\frac{\bar{u}\bar{v}}{\bar{S}_u^2} - \sqrt{g(\bar{u},\bar{v},\bar{S}_u)}}{\left(\left(\frac{\bar{v}}{\bar{S}_u}\right)^2 - 1\right)} \quad \frac{\partial\bar{\zeta}}{\partial r}(z,r) = \frac{\frac{\bar{u}\bar{v}}{\bar{S}_u^2} + \sqrt{g(\bar{u},\bar{v},\bar{S}_u)}}{\left(\left(\frac{\bar{v}}{\bar{S}_u}\right)^2 - 1\right)} \quad (6)$$

where g is defined as $g(\bar{u},\bar{v},\bar{S}_u) = \left(\frac{\bar{u}\bar{v}}{\bar{S}_u^2}\right)^2 - \left(\left(\frac{\bar{v}}{\bar{S}_u}\right)^2 - 1\right)\left(\left(\frac{\bar{u}}{\bar{S}_u}\right)^2 - 1\right)$. Given that the steady state slope of the flame surface is now not simply linear, as is the case for uniform flow, it is difficult to solve analytically, but can easily be integrated numerically to give the steady state flame positions shown in Fig. 2.

The boundary conditions are chosen such that the flame surfaces always remain attached to the flame holder: $\xi(a,t) = 0$ and $\zeta(b,t) = 0$. In this study, the velocity fluctuations do not approach the magnitude of the mean flow, and the discontinuous boundary conditions proposed by Dowling [1] and others are not required.

Time Delays

Previous studies (Lieuwen & Zinn [39], Cho & Lieuwen [3]) have noticed that where fluctuations in equivalence ratio ϕ occur, they are often the dominant mechanism of unsteady heat release, affecting both the flame speed S_u and the enthalpy of combustion ΔH . These fluctuations are then assumed to convect downstream with the bulk flow velocity to the flame front where combustion occurs. At this point, the equivalence ratio is calculated as

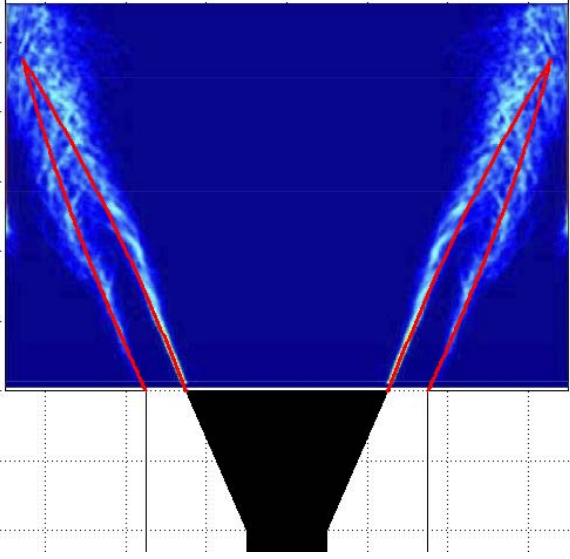


FIGURE 2. STEADY STATE FLAME POSITION OVERLAID ON CHEMILUMINESCENCE IMAGE (FROM [4]), FLOW CONDITIONS $\|\bar{u}\| = 10\text{m/s}$, $\bar{\phi} = 0.55$

$\phi(r, \xi, t) = \phi_0(t - \tau(r, \xi, t))$, where $\phi_0(t)$ is the equivalence ratio at the location of fuel injection. This convection time delay τ is therefore critical in determining the dynamic response of the flame. Two difference approximations are considered for calculating this time delay:

Varying-in-space, Constant-in-time - the fluctuations of equivalence ratio at the fuel injection point are convected by the *mean* flow velocity downstream to the *steady-state* flame position. Due to the inclined flame positions, this leads to a time delay which is constant in time, but varies with radial position. The geometry is divided into three sections: the combustor, the neck (past the flame holder), and the inflow pipe, with a convection time delay associated with each. The flow in the latter two sections is assumed to be axial, and determined by continuity. In the first section (combustor), we express the total convection distance to be $\rho_{conv} = \sqrt{r^2 + (L + \xi(r))^2} \left(1 - \frac{L}{L + \xi(r)}\right)$, where ρ is the spherical radial coordinate. This is simply the distance travelled by the flow between the inlet to the combustor and the steady-state position of the flame surface. Therefore, the time delay is the result of the integral:

$$\overline{\tau_3(r, \xi)} = \int_0^{\rho_{conv}} \frac{1}{u_\rho} d\rho \quad \text{where} \quad u_\rho = \frac{-A}{\rho^2} \quad (7)$$

Similarly, for the time delay associated with flow past the flame holder. In this case the convection distance is given by $z_2 =$

$\frac{a-d}{\tan(\alpha)}$, where α is the cone angle of the flame holder. The flow is assumed to be axial and governed by continuity, Therefore, as before we can write:

$$\overline{\tau_2} = \int_0^{z_2} \frac{1}{u_2} dz \quad \text{where} \quad u_2 = \frac{\bar{u}_G(b^2 - a^2)}{b^2 - z^2 \tan^2(\alpha)} \quad (8)$$

Finally for the inflow pipe, the convection distance is taken to be $z_1 = L_{inj} - \frac{(a-d)}{\tan(\alpha)}$, where L_{inj} is defined as the distance from the fuel injection point to the dump plane. In this case, there is no area variation, and therefore the convection velocity is uniform, and given by $u_1 = \frac{u_G(b^2 - a^2)}{(b^2 - d^2)}$. Therefore, the time delay $\overline{\tau_1}$ is simply the convection distance divided by the convection speed, giving:

$$\overline{\tau_1} = \frac{b^2 - d^2}{\bar{u}_G(b^2 - a^2)} \left[L_{inj} - \frac{(a-d)}{\tan(\alpha)} \right] \quad (9)$$

The total steady-state time delay is simply the sum of these three components: $\tau(r, \xi) = \tau_3(r, \xi) + \overline{\tau_2} + \overline{\tau_1}$. The procedure for the second flame surface ζ is identical, so is not detailed here.

Varying-in-space, Varying-in-time - The previous model gives a good estimate of the time delays involved for small perturbations of velocity and flame front location. However, it is obvious both from experimental data [5], and from examining the results of this model, that these assumptions are difficult to justify at larger perturbation amplitudes. At these higher amplitudes, the flame front deviates significantly from the steady-state position, changing the convection distance and hence the time delay. In this model the time delays are calculated using the convection distance to the *instantaneous* flame position, and using the *fluctuating* flow velocity from previous timesteps to calculate the convection velocity. The convection distance only varies within the combustor, where it becomes $\rho_{conv}(r, t) = \sqrt{r^2 + (L + \xi(r, t))^2} \left(1 - \frac{L}{L + \xi(r, t)}\right)$, where ρ is the spherical radial coordinate, and L is the distance between the origin of the radial flow streamlines and the dump plane. $\xi(r, t)$ is now the instantaneous flame surface position (the same procedure is followed for the second flame surface ζ , so is not detailed in full here).

Starting with the differential equation for convection distance:

$$\frac{\partial \rho}{\partial t} = u_\rho(\rho, t) = \frac{-A(t)}{\rho^2} \quad (10)$$

Rearranging and integrating both sides then gives:

$$\frac{\rho^3}{3} = - \int_{t-\tau_3(\rho,t)}^t A(t') dt'. \quad (11)$$

At this point there are two possible ways of solving for the time delay $\tau_3(\rho, t)$. In the first case, the current flame position and velocity field can be used to calculate the position of the equivalence ratio ‘packet’ currently being burnt in the previous timestep. This can then be repeated, tracking the equivalence ratio ‘packet’ backwards in time to its exit from the fuel injector. An approach similar to this has been followed successfully in the past (e.g. Stow and Dowling [44]), but increases the computational cost of the model.

An alternative approach is to differentiate Eqn. (11) with respect to time to arrive at the following partial differential equation:

$$\begin{aligned} (L + \xi) \frac{\partial \xi}{\partial t} \left[\sqrt{(L + \xi)^2 + r^2} - 2\rho_{inj} + \frac{\rho_{inj}^2}{\sqrt{(L + \xi)^2 + r^2}} \right] \\ = -A(t) + A(t - \tau_3) \left[1 - \frac{\partial \tau_3}{\partial t} \right] \end{aligned} \quad (12)$$

and then rearrange to give

$$\frac{\partial \tau_3}{\partial t} = 1 - \frac{A(t) + (L + \xi) \left[\sqrt{(L + \xi)^2 + r^2} - 2\rho_{inj} + \frac{\rho_{inj}^2}{\sqrt{(L + \xi)^2 + r^2}} \right] \frac{\partial \xi}{\partial t}}{A(t - \tau_3)} \quad (13)$$

A similar approach can be used to calculate the time delays τ_2 and τ_1 .

This PDE can then be solved along with the flame surface equation at each time step, using the flame surface and time delays calculated at the previous time step. This approach offers the advantage of being computationally efficient, and fitting well with the set of flame surface PDEs. However this approach can have difficulties describing the abrupt changes in time delay associated with the wrinkling and pinch-off of the flame surface. The calculation of the time delay requires knowledge of the historical and current flame surface position. As this is only known at discrete time-steps, the intermediate time-steps necessary for higher-order solvers are not available. Therefore, the solution of these PDEs is limited to a first order solver. As the flame surface becomes highly wrinkled, and occasionally pinches off, the time delay at some points on the flame surface may vary sufficiently quickly that a first order scheme has difficulty accurately

Dimension	Value	Constant	Value
a	12.5mm	η	1
b	17.5mm	ρ_u	1.2
c	35mm	k_0	1.51314
d	4mm	k_1	1.32176
L	40mm	k_2	3.11023
L_{inj}	55mm	k_3	1.72307
α	45°	k_4	0.36196

TABLE 1. Dimensions and constant values used

capturing this behaviour.

FLAME MODEL RESULTS

The flame model has been run on the same geometry (see Fig. 1 & 8), and with the same operating conditions used by Balachandran et al. [5]. The fuel is ethylene, the mean equivalence ratio $\bar{\phi}$ is 0.55, and the mean velocity at the dump plane \bar{u}_G is 10 m/s. Table 1 gives values for the various dimensions and constants used. The enthalpy of combustion is given by $\Delta H(\phi) = \frac{3.2 \min(\phi, 1)}{(1+0.067\phi)} \text{ MJ kg}^{-1}$. The rig can either be run in a ‘fully premixed’ mode, where mixing occurs far upstream and equivalence ratio is constant, or in an ‘imperfectly premixed’ mode, where the fuel is injected downstream of the plenum, 55mm upstream of the dump plane. In this configuration equivalence ratio varies temporally as a result of the velocity fluctuations past the fuel injection point. This coupling is taken to be dictated by continuity and takes the form:

$$\phi_0 = \frac{\bar{u}_G \bar{\phi}_0}{u_G} \quad (14)$$

Loudspeakers provide the means of acoustic forcing. To investigate the forced response, the combustor length was kept sufficiently short to ensure that the rig did not self-excite.

The model was run for a frequency range between 5 and 500 Hz, and for forcing amplitudes V between 1% and 40%. In the forced calculations, $u_G(t) = \bar{u}_G(1 + V \sin(\omega t))$. The model is run for approximately 15 cycles of the forcing frequency. Transient effects disappear after about 3 cycles, and the characteristics of the flame are analysed thereafter. The time-step used was 10^{-5} seconds, and the model was run for both the time-varying and constant time delay models. However, the results presented in this section were obtained using the time-varying time delay method exclusively, as this uses more realistic assumptions at higher levels of forcing.

A first indication of the model's behaviour will be the evolution of the flame surface. The variation in flame area is expected to be a major mechanism for producing perturbations in heat release. Wrinkling of the flame front can be produced both by fluctuations in the velocity field, and fluctuation of the flame speed due to changes in equivalence ratio. This model finds that the effect of velocity perturbations is noticeably weaker than that of equivalence ratio perturbations, except at very low frequencies (< 40 Hz). This is consistent with many experimental and analytical results (e.g. Richards & Janus [45], Balachandran [4], Cho & Lieuwen [3]) on systems with varying equivalence ratios. In perfectly premixed systems when the equivalence ratio is always constant emphasis is placed on the weaker effects of the unsteady velocity field on flame area. Then it is found that vorticity has a significant effect on flame area changes. Since vorticity is not accounted for in this model, this causes some differences between modelled and experimental results for perfectly premixed systems. However, in the case of temporally varying equivalence ratio operating conditions, the wrinkling of the flame by equivalence ratio fluctuations is the dominant mechanism of unsteady heat release. Figure 3 shows the progression of the flame surfaces under equivalence ratio and velocity forcing of the form seen in Eqn. (14) at four points in the cycle. The equivalence ratio variations are shown by the contours. The flame surface shows some realistic characteristics such as cusping and flame surface intersection leading to multiple combustion zones and burn-off. The wrinkling effect of the equivalence ratio variations is also evident. As an area of richer fuel (red colour) is convected down the flame, the flame speed accelerates, drawing the flame surfaces closer together. They can meet, and for higher amplitudes of forcing pinch off part of the flame, which then burns more slowly in an area of relatively lean mixture. At higher frequencies than that shown in Fig. 3, the equivalence ratio fluctuations are spatially closer, the flame surfaces become wrinkled with a correspondingly smaller wavelength and an amplitude insufficient to pinch off except near the flame tip.

The fluctuating heat release is calculated, as in Eqn. 3, from the instantaneous flame area, local flame speed and enthalpy of combustion. This is then compared against experimental heat fluctuations measured by OH^* and CH^* chemiluminescence, as well as flame surface density measurements based on OH PLIF data carried out by Balachandran [5]. At low levels of acoustic forcing the unsteady heat release $Q'(t)$ is sinusoidal in nature. However, at higher levels of forcing, the nonlinear nature of the strongly wrinkled flame fronts becomes quickly apparent. Figure 4 illustrates the good agreement between the G-Equation model and experiment, both in terms of the loop-shape of the oscillation and its magnitude. The sharp peaks in heat release in this case correspond to the necking and subsequent intersection of the two flame surfaces, leading to rapid changes in the flame surface area.

The variation of both Q'/\bar{Q} and Flame Transfer Function

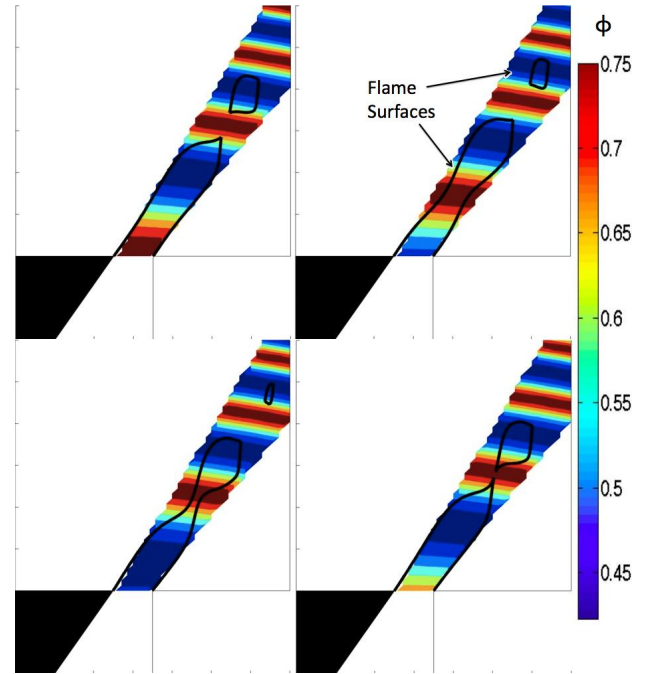


FIGURE 3. FLAME SURFACE EVOLUTION AT 150HZ AND 30% FORCING, SHOWING THE EFFECT OF EQUIVALENCE RATIO FLUCTUATIONS

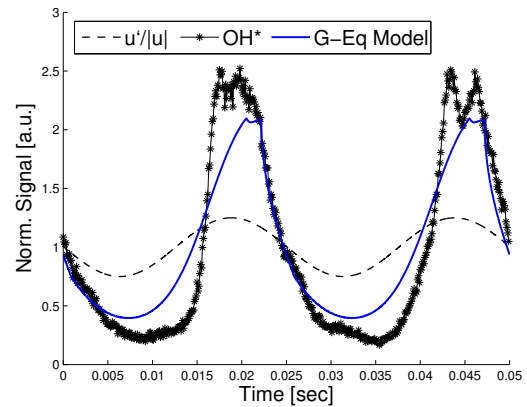


FIGURE 4. COMPARING UNSTEADY HEAT RELEASE FROM EXPERIMENT USING OH^* CHEMI-LUMINESCENCE AND G-EQUATION MODEL AT 40Hz AND 25% FORCING

$H = \frac{Q'/\bar{Q}}{u'/\bar{u}}$ with forcing level and frequency is also compared with experiment (Fig. 5 and 7). Figure 5 shows good agreement between the experiment and the G-equation model for a range of forcing amplitudes at 160Hz.

At low frequencies, an investigation of the model behaviour shows that the part of the FTF which relates to velocity perturbations u' , and the part which relates only to equivalence ratio

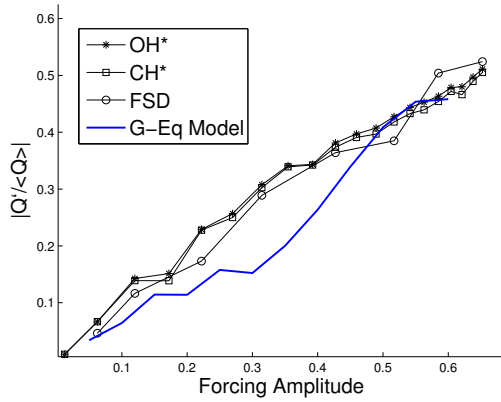


FIGURE 5. COMPARING THE VARIATION OF Q'/\bar{Q} WITH FORCING AMPLITUDE FROM EXPERIMENT USING OH*, CH* CHEMILUMINESCENCE AND FLAME SURFACE DENSITY MEASUREMENTS [5] AND G-EQUATION MODEL AT $160Hz$

effects ϕ' , both tend to unity, with a phase difference of π between them (Fig. 6). From quasi-steady state arguments, this seems reasonable, as in this case the mass flow rate of fuel is constant. Therefore, the fluctuations in equivalence ratio are a result of fluctuations in fluid flow at the fuel injection point, and thus tend to be proportional to, and out of phase with, the velocity fluctuations (similar to the *stiff fuel injection system* case discussed by Polifke & Lawn [46]). As such the total modelled FTF tends to zero at very low frequencies.

Figure 7 compares the calculated FTF plotted against frequency with experiment for a variety of forcing amplitudes. The decaying oscillatory nature of the gain is well captured. The experimental FTF appears to tend to a maximum as frequency tends toward zero. However, this is based on u' measurements made using the two microphone technique, which becomes increasingly inaccurate at low frequencies. The phase plot of the calculated FTF shows some interesting behaviour, with two separate regimes being seen. The first, present at low forcing amplitudes up to 14%, is characterised by a quicker phase roll-off at frequencies above $100Hz$ than observed in experiment. The second regime, observed at higher amplitudes of forcing, exhibits a much slower phase roll-off at high frequencies, closer to that observed by experiment. The transition between these two regimes seems to be associated with the onset of flame surface intersections and flame pinch off.

COUPLING OF THE ACOUSTIC AND COMBUSTION PROCESSES

In order to be useful in predicting the onset and amplitude of thermo-acoustic oscillations, the flame model developed must be combined with a model of the acoustics of the combustor in order to model the closed-loop system. In order to investigate the

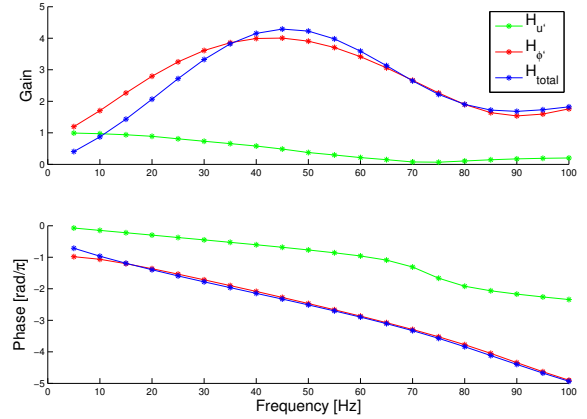


FIGURE 6. FLAME TRANSFER FUNCTION GAIN & PHASE, ILLUSTRATING THE RELATIVE IMPORTANCE OF VELOCITY ($H_{u'}$) AND EQUIVALENCE RATIO ($H_{\phi'}$) PERTURBATIONS

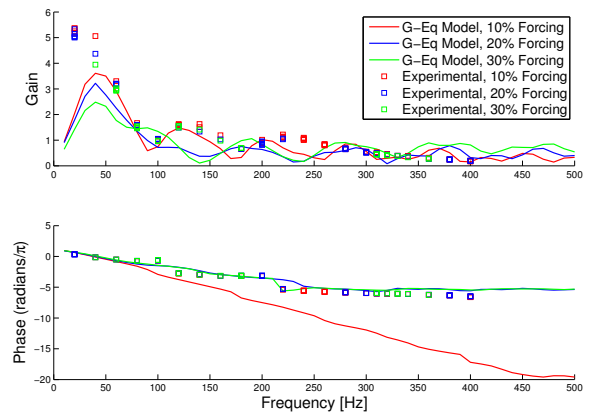


FIGURE 7. VARIATION OF FLAME TRANSFER FUNCTION GAIN & PHASE WITH FREQUENCY FROM EXPERIMENT AND G-EQUATION MODEL

self-excited behaviour, the combustor length was extended, and no external forcing was used. When operated in premixed mode the rig was not found to self-excite. However, when operated in the ‘imperfectly premixed’ mode a self-excited thermo-acoustic oscillation was recorded. Thus, this analysis will focus on this operating condition. The acoustics of the combustor have been modelled in a 1D acoustic network model called LOTAN developed by Stow & Dowling [44]. This model uses linear theory to predict combustion oscillations (described in full in Dowling & Stow [47]). Using nonlinear flame models it can also give limit cycle amplitude predictions (Stow & Dowling [48]). However, the nonlinear combustion models currently available are basic saturation models with simple time delays. When a nonlinear

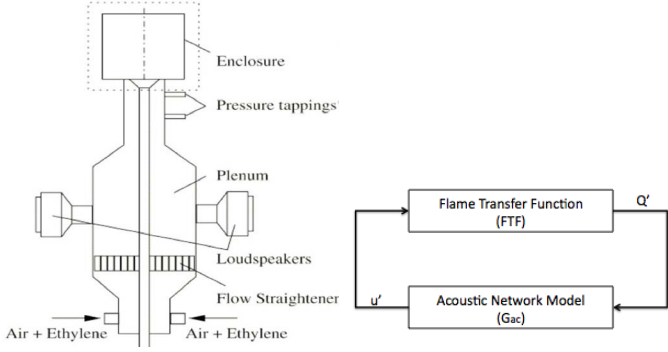


FIGURE 8. SCHEMA OF EXPERIMENTAL RIG AND BLOCK DIAGRAM OF CLOSED FEEDBACK LOOP

model is used the combustion zone is assumed to be the only source of nonlinearity, with the flow elsewhere behaving linearly.

Linear Analysis

In the first instance a purely linear analysis can reveal which modes are unstable, and hence liable to be self-excited. A flame transfer function $H(\omega)$ calculated from the G-equation model (as in Fig.7, but at 3% forcing to ensure linear behaviour) is fitted by an analytical function comprising a ratio of complex polynomials of the form:

$$H_{linear}(i\omega) = \frac{a_n(i\omega)^n + a_{n-1}(i\omega)^{n-1} + \dots + a_1(i\omega) + a_0}{b_n(i\omega)^n + b_{n-1}(i\omega)^{n-1} + \dots + b_1(i\omega) + b_0} \quad (15)$$

LOTAN can be used in the frequency domain with a specified FTF to determine the complex frequencies at which the downstream boundary condition is satisfied, indicating the eigenfrequencies and modes of the system. The real part of the eigenfrequency determines the frequency of a self-excited oscillation, and the imaginary part corresponds to the growth rate, with a positive growth rate indicating an unstable mode. Using this method with the flame transfer function for perfectly premixed combustion, we find that all modes are stable. Experiments by Balachandran [4] also found no self-excited modes in this condition. However, when the FTF calculated with temporally varying equivalence ratio is used, a mode at 345Hz becomes unstable. Figure 9 is a Bode Plot showing the gain and phase of the linear closed loop transfer function (CLTF). At 3% forcing, the peak visible at 345Hz in the gain plot is accompanied by a 180° increase in phase, indicating the presence of a double unstable pole. This corresponds well with the unstable oscillation at 348Hz noted in experiments [4].

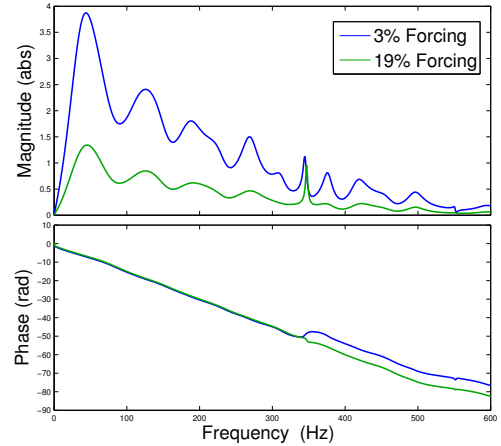


FIGURE 9. BODE PLOT SHOWING THE GAIN AND PHASE OF THE CLOSED LOOP TRANSFER FUNCTION WITH 3% AND 19% FORCING

Describing Function Analysis

In order to investigate this mode further, a describing function is used to reflect the saturation of the flame model at this frequency (a similar approach to that of Noiray et al. [49]). A function $K(\omega, A)$ is defined as the ratio between the linear FTF and nonlinear FTF calculated at an amplitude A using the G-equation approach previously described.

$$K(\omega, A) = \frac{H_{nonlinear}(\omega)}{H_{linear}(\omega)} \quad (16)$$

$K(\omega, A)$ is complex since it is clear from Fig. 7 that there is a change both in magnitude and phase of the FTF with amplitude A . The acoustic network model is used to output an acoustic transfer function $G_{ac}(\omega)$ between unsteady heat release and unsteady velocity at the inlet to the combustor (see Fig. 8). The closed loop transfer function can therefore be expressed as:

$$CLTF = \frac{K(\omega, A)H(\omega)}{1 + K(\omega, A)H(\omega)G_{ac}(\omega)} \quad (17)$$

The pole of the CLTF determines the frequency and growth rate of disturbances of amplitude A . At small amplitudes we have seen the that the system is unstable. The amplitude of the oscillation can be ‘increased’, altering the flame transfer function until saturation occurs and the growth rate become zero, stabilising the system and thereby indicating the amplitude of a limit cycle.

Using this technique it is found that the unstable mode at 345Hz is predicted to reach a limit cycle with an amplitude of

19%, the second case seen in Fig. 9. This compares well with experimental observations, where the same unstable mode reached a limit cycle amplitude of 21%.

Nonlinear Time Domain Analysis

While both these methods are useful in predicting the frequency, stability, and possible limit cycle amplitudes of the unstable modes, neither can reproduce the full nonlinear behaviour, when different modes may interact. In order to fully model the development of the self-excited oscillation, the flame model must be run in the time domain with acoustic feedback. The ‘acoustic’ transfer function $G_{ac}(\omega)$ describes the linear waves produced by a harmonic fluctuation in the rate of heat release determined by the network model. This is converted to the corresponding time-domain Green function by taking the inverse Fourier transform:

$$A = \frac{u_G(t)}{u_G} = \int G_{ac}(t - \tau) \frac{Q(\tau)}{Q} d\tau \quad (18)$$

A full description of this approach can be found in Stow & Dowling [50]. The flame model used is the same heat release model as described in Eqn. 3, with the flame position based on solving the G-Equation in a known velocity field. The steady velocity field is given by the analytical solution described above. However, the normalised amplitude of the velocity perturbations $A(t)$, previously used to implement sinusoidal forcing, is now found by coupling the ‘acoustic’ Green function with current and previous values of heat release as shown in Eqn. 18. This thus provides closure to the feedback loop.

The G-Equation flame model is first run in the time domain with no forcing or coupling to give a steady solution. After any transients decay, the flame model is coupled with the acoustic Green function in the manner described. The closed system is initially given a small broadband perturbation and then allowed to evolve. The self-excited oscillations are allowed to develop until the nonlinearity in the combustion process causes it to enter a limit cycle. That stable limit cycle (shown in Fig. 10) develops at the dominant frequency of $357Hz$, the same unstable mode observed previously. The limit cycle amplitude is 23%. This agrees well with the experimental observations of Balachandran [4], which recorded a dominant mode at $348Hz$ and 21%.

CONCLUSIONS

In this paper a flame model based on the kinematic G-equation has been developed. The model consists of two interacting flame surfaces, and uses a nonuniform spreading flow, and can be run with either a constant or temporally varying equivalence ratio. Two approximations for the convection time delays associated with the equivalence ratio fluctuations have been proposed; one based on the steady state flame positions and con-

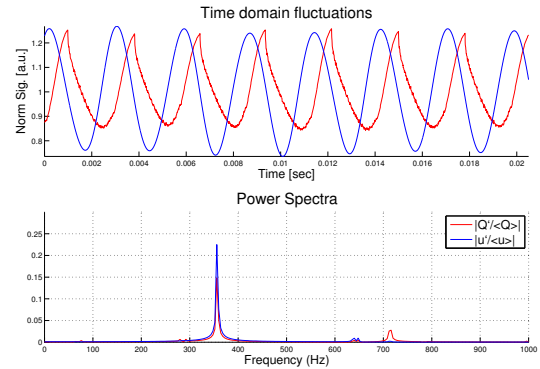


FIGURE 10. TIME DOMAIN AND FREQUENCY SPECTRUM OF LIMIT CYCLE OSCILLATION AT $357Hz$

vection velocities, and a second calculated using instantaneous values.

This model has been run with acoustic forcing for a large range of frequencies and forcing amplitudes. The flame surfaces exhibit realistic behaviour seen in experiment such as cusping and pinch-off. The temporal evolution of heat release is also in good agreement with experiments. The gain of the calculated flame transfer function agrees well with experiments, with the time-varying time delay model providing slightly better agreement. The agreement is not quite as good for the phase of the calculated FTF, which displays a faster phase roll-off at low forcing amplitudes which was not captured by experiments.

The flame model developed has been coupled with a linear wave network model in order to investigate the interaction between the acoustic and combustion processes. A linear coupling finds an unstable resonant mode at around $345Hz$, as observed by experiment. The saturation of the combustion process has been modelled both by means of a describing function, and by running the flame model in the time domain using a Green function to represent the acoustics of the closed loop system. This approach predicts a limit cycle which is in very good agreement with experimental observations.

ACKNOWLEDGMENT

The authors are grateful to the EC for the support for the present work, performed within the Marie Curie RTN project AETHER (Contract No. MRTN-CT-2006-035713).

REFERENCES

- [1] Dowling, A., 1999. “A kinematic model of a ducted flame”. *Journal of fluid mechanics*, **394**, pp. 51–72.
- [2] Schuller, T., Ducruix, S., Durox, D., and Candel, S., 2002. “Modeling tools for the prediction of premixed flame transfer functions”. *Proceedings of the Combustion Institute*, **29**(1), pp. 107–113.

- [3] Cho, J., and Lieuwen, T., 2005. “Laminar premixed flame response to equivalence ratio oscillations”. *Combustion and Flame*, **140**(1-2), pp. 116–129.
- [4] Balachandran, R., 2005. “Experimental investigation of the response of turbulent premixed flames to acoustic oscillations”. *PhD Thesis, University of Cambridge*.
- [5] Balachandran, R., Ayoola, B., Kaminski, C., Dowling, A., and Mastorakos, E., 2005. “Experimental investigation of the nonlinear response of turbulent premixed flames to imposed inlet velocity oscillations”. *Combustion and Flame*, **143**(1-2), pp. 37–55.
- [6] Candel, S., 2002. “Combustion dynamics and control: Progress and challenges.”. *Proceedings of the Combustion Institute*, **28**, Feb, pp. 1–28.
- [7] Lieuwen, T., 2003. “Modeling premixed combustion-acoustic wave interactions: A review”. *Journal of Propulsion and Power*, **19**(5), pp. 765–781.
- [8] Lieuwen, T., 2002. “Experimental investigation of limit-cycle oscillations in an unstable gas turbine combustor”. *Journal of Propulsion and Power*, **18**(1), pp. 61–67.
- [9] Giuliani, F., Gajan, P., Diers, O., and Ledoux, M., 2002. “Influence of pulsed entries on a spray generated by an air-blast injection device: An experimental analysis on combustion instability processes in aeroengines”. *Proceedings of the Combustion Institute*, **29**(1), pp. 91–98.
- [10] Bloxside, G., Dowling, A., and Langhorne, P., 1988. “Re-heat buzz: an acoustically coupled combustion instability. part 2. theory”. *Journal of fluid mechanics*, **193**, pp. 445–473.
- [11] Candel, S., Durox, D., and Schuller, T., 2004. “Flame interactions as a source of noise and combustion instabilities”. *10th AIAA/CEAS Aeroacoustics Conference AIAA 2004-2928*.
- [12] Williams, J., 1984. “Review lecture: Anti-sound”. *Proceedings of the Royal Society of London. Series A Mathematical and Physical Sciences*, **395**(1808), Sep, pp. 63–88.
- [13] Rayleigh, J., 1896. “The theory of sound, vol 2.”. *Dover Publications*.
- [14] Merk, H., 1956. “An analysis of unstable combustion of premixed gases”. *Sixth Symposium (International) on Combustion 500-512 Pittsburgh Pennsylvania: The Combustion Institute*.
- [15] Blackshear, P., 1952. “Driving standing waves by heat addition”. *National Advisory Committee on Aeroacoustics, Technical Note 2772*.
- [16] Matsui, Y., 1981. “An experimental study on pyro-acoustic amplification of premixed laminar flames”. *Combustion and Flame*, **43**(1), pp. 199–209.
- [17] Poinsot, T., Trouve, A., Veynante, D., Candel, S., and Eposito, E., 1987. “Vortex-driven acoustically coupled combustion instabilities”. *Journal of fluid mechanics*, **177**, pp. 265–292.
- [18] Yu, K., Trouvé, A., and Daily, J., 1991. “Low-frequency pressure oscillations in a model ramjet combustor”. *Journal of fluid mechanics*, **232**, pp. 47–72.
- [19] Paschereit, C. O., Gutmark, E., and Weisenstein, W., 2000. “Excitation of thermoacoustic instabilities by interaction of acoustics and unstable swirling flow”. *AIAA Journal*, **38**(6), pp. 1025–1034.
- [20] Baillot, F., Durox, D., and Prud’Homme, R., 1992. “Experimental and theoretical study of a premixed vibrating flame”. *Combustion and Flame*, **88**(2), pp. 149–152.
- [21] Birbaud, A., Durox, D., Ducruix, S., and Candel, S., 2007. “Dynamics of confined premixed flames submitted to upstream acoustic modulations”. *Proceedings of the Combustion Institute*, **31**(1), pp. 1257–1265.
- [22] Durox, D., Schuller, T., and Candel, S., 2005. “Combustion dynamics of inverted conical flames”. *Proceedings of the Combustion Institute*, **30**(2), pp. 1717–1724.
- [23] Palies, P., Durox, D., Schuller, T., and Candel, S., 2010. “The combined dynamics of swirler and turbulent premixed swirling flames”. *Combustion and Flame*, **157**(9), Sep, pp. 1698–1717.
- [24] Fritsche, D., Furi, M., and Boulouchos, K., 2007. “An experimental investigation of thermoacoustic instabilities in a premixed swirl-stabilized flame”. *Combustion and Flame*, **151**(1-2), pp. 29–36.
- [25] Kopp-Vaughan, K. M., Tuttle, S. G., Renfro, M. W., and King, G. B., 2009. “Heat release and flame structure measurements of self-excited acoustically-driven premixed methane flames”. *Combustion and Flame*, **156**(10), Oct, pp. 1971–1982.
- [26] Hield, P. A., Brear, M. J., and Jin, S. H., 2009. “Thermoacoustic limit cycles in a premixed laboratory combustor with open and choked exits”. *Combustion and Flame*, **156**(9), Sep, pp. 1683–1697.
- [27] Altay, H. M., Speth, R. L., Hudgins, D. E., and Ghoniem, A. F., 2009. “The impact of equivalence ratio oscillations on combustion dynamics in a backward-facing step combustor”. *Combustion and Flame*, **156**(11), Nov, pp. 2106–2116.
- [28] Auer, M., Hirsch, C., and Sattelmayer, T., 2005. “Influence of the interaction of equivalence ratio and mass flow fluctuations on flame dynamics”. *ASME Turbo Expo: Power for Land, Sea, and Air: GT2005-68373*, pp. 249–257.
- [29] Auer, M., Hirsch, C., and Sattelmayer, T., 2006. “Influence of air and fuel mass flow fluctuations in a premix swirl burner on flame dynamics”. *ASME Turbo Expo: Power for Land, Sea, and Air: GT2006-90127*, pp. 97–106.
- [30] Kim, K. T., Lee, J., Lee, H. J., Quay, B. D., and Santavicca, D., 2008. “Flame transfer function measurement and instability frequency prediction using a thermoacoustic model”. *Proceedings of ASME Turbo Expo 2009(GT2009-60026)*, Nov, pp. 1–11.

- [31] Lee, H., Kim, K., Lee, J., Quay, B., and Santavicca, D. A., 2009. "An experimental study on the coupling of combustion instability mechanisms in a lean premixed gas turbine combustor". *ASME Turbo Expo: Power for Land, Sea, and Air. GT2009-60009*, pp. 749–758.
- [32] Fleifil, M., Annaswamy, A., Ghoneim, Z., and Ghoniem, A., 1996. "Response of a laminar premixed flame to flow oscillations: A kinematic model and thermoacoustic instability results". *Combustion and Flame*, **106**(4), pp. 487–510.
- [33] Ducruix, S., Schuller, T., Durox, D., and Candel, S., 2003. "Combustion dynamics and instabilities: Elementary coupling and driving mechanisms". *Journal of Propulsion and Power*, **19**(5), pp. 722–734.
- [34] Lieuwen, T., 2005. "Nonlinear kinematic response of premixed flames to harmonic velocity disturbances". *Proceedings of the Combustion Institute*, **30**(1), pp. 1725–1732.
- [35] Palies, P., Schuller, T., Durox, D., and Candel, S., 2011. "Modeling of premixed swirling flames transfer functions". *Proceedings of the Combustion Institute*, **33**, pp. 2967–2974.
- [36] Keller, J., 1995. "Thermoacoustic oscillations in combustion chambers of gas turbines". *AIAA Journal*, **33**(12), pp. 2280–2287.
- [37] Hubbard, S., and Dowling, A., 1998. "Acoustic instabilities in premix burners". *4th AIAA/CEAS Aeroacoustics Conference (19th AIAA Aeroacoustics Conference) AIAA-1998-2272*.
- [38] Hubbard, S., and Dowling, A., 2001. "Acoustic resonances of an industrial gas turbine combustion system". *Journal of Engineering for Gas Turbines and Power*, **123**(4), Jan, pp. 766–773.
- [39] Lieuwen, T., and Zinn, B., 1998. "The role of equivalence ratio oscillations in driving combustion instabilities in low nox gas turbines". *Symposium (International) on Combustion*, **27**(2), pp. 1809–1816.
- [40] Hemchandra, S., Shreekrishna, and Lieuwen, T., 2007. "Premixed flame response to equivalence ratio perturbations". *ASME/ASME/AIAA Joint Propulsion Conference, Cincinnati OH, AIAA 2007-5656*.
- [41] You, D., Huang, Y., and Yang, V., 2005. "A generalized model of acoustic response of turbulent premixed flame and its application to gas-turbine combustion instability analysis". *Combustion Sci. & Tech.*, **177**(5-6), pp. 1109–1150.
- [42] Abu-Orf, G., 1996. "Laminar flamelet reaction rate modelling for spark-ignition engines." *PhD Thesis, University of Manchester Institute of Science and Technology, Manchester, UK*.
- [43] White, F., 2005. *Fluid Mechanics, 5th Ed., McGraw Hill*.
- [44] Stow, S., and Dowling, A., 2001. "Thermoacoustic oscillations in an annular combustor". *Proceedings of ASME TURBO EXPO, 2001-GT-0037*, Jun.
- [45] Richards, G. A., and Janus, M. C., 1998. "Characterization of oscillations during premix gas turbine combustion". *Journal of Engineering for Gas Turbines and Power*, **120**(2), p. 294.
- [46] Polifke, W., and Lawn, C., 2007. "On the low-frequency limit of flame transfer functions". *Combustion and Flame*, **151**(3), pp. 437–451.
- [47] Dowling, A., and Stow, S., 2003. "Acoustic analysis of gas turbine combustors". *Journal of Propulsion and Power*, **19**(5), pp. 751–764.
- [48] Stow, S., and Dowling, A., 2004. "Low-order modelling of thermoacoustic limit cycles". *Proceedings of ASME TURBO EXPO GT2004-54245*, Jun.
- [49] Noiray, N., Durox, D., Schuller, T., and Candel, S., 2008. "A unified framework for nonlinear combustion instability analysis based on the flame describing function". *Journal of Fluid Mech.*, **615**, pp. 139–167.
- [50] Stow, S., and Dowling, A., 2009. "A time-domain network model for nonlinear thermoacoustic oscillations". *Journal of Engineering for Gas Turbines and Power*, **131**, p. 031502.